Spin-Orbit Coupling in Diamond and Zincblende Heterostructures

Miguel A. Oliveira* and Angus MacKinnon
Blackett Laboratory, Imperial College London, South Kensington Campus, London SW7 2AZ, UK†
(Dated: February 2, 2008)

Spin splittings in III-V materials and heterostructures are of interest because of potential applications, mainly in spintronic devices. A necessary condition for the existence of these spin splittings is the absence of inversion symmetry. In bulk zincblende materials the inversion symmetry is broken, giving rise to a small spin splitting. The much larger spin splitting observed in quantum wells is normally attributed to the asymmetry of the confining potential and explained on the basis of the Rashba effect. For symmetrically confined wells, where the only source of asymmetry is that of the underlying crystal potential, the confining potential strongly enhances the spin splittings. This enhancement does not require the asymmetry of the confining potential but depends on the interplay between the confinement and the crystal potential. In this situation the behavior of the spin splittings is consistent with the Dresselhaus contribution.

In asymmetrically confined wells both Dresselhaus and Rashba terms contribute.

We present a general theory of the spin splittings of these structures based on the group theory of diamond and zincblende heterostructures.

I. INTRODUCTION

Spin is one of the most intriguing properties of subatomic particles and its explanation is among the most significant achivements of quantum theory. Although the field of electronics has taken full advantage of electronic charge, spin has been relatively unexploited in any practical application with the noteable exception of magnetic read heads based on giant magnetoresistance. However recent developments suggest that this is about to change. The new field of spintronics[1] is steadily growing with the aim of taking full advantage of spin as well as charge. Some devices have been already proposed[2,3] and some experimental work[4] is already taking advantage of some basic spin properties of heterostructures.

However the spin properties of heterostructures of IV and III-V materials are still not completely understood. In spite of recent advances,[5,6] no detailed atomistic simulations are yet available (to our knowledge) on the spin properties of the materials that form the backbone of the semiconductor industry. Most of the work reported in the literature relates to a particular form of the $\vec{k}\cdot\vec{p}$ model.[5,6] It is only recently that this model has been able to incorporate the full symmetries of these heterostructures.[5]

We shall present a method of predicting the spin splittings of these structures and we shall present results based on the Empirical Pseudopotential Layer Method (EPLM) that corroborate our claims. The often discussed contributions of bulk inversion asymmetry (BIA) and structural inversion asymmetry (SIA) will be presented as consequences of the symmetries of the heterostructure and we shall show clearly that any detailed calculation must include both.

Section II will contain a summary description of the computational methods. Section III will focus on the consequences of symmetry for the spin splittings of these structures. The following sections contain a discussion of our results followed by section VII where conclusions will be drawn.

II. THE COMPUTATIONAL MODELS

The EPLM has already been discussed elsewhere[7] so we shall only describe it here briefly, mainly to point out the particulars of our implementation.

In a conventional band structure calculation a set of eigenenergies is calculated for a particular value of the wavevector, $\vec{k}$. By contrast a scattering approach, such as EPLM, works with a fixed energy and $\vec{k}_{\parallel}$ parallel to an interface and calculates a set of solutions for $k_{\perp}$ perpendicular to that interface. These solutions include examples with real and complex $k_{\perp}$, often called the *complex* band structure. Solutions for different layers may be combined using appropriate matching conditions to generate solutions for more complicated combinations of layers. Typically the result may be expressed as a transmission coeficient for the multi–layer system. Eigenstates of the system then manifest themselves as resonances in the transmission coefficient or as bound states decaying into the gap of the embedding material.

We also consider a much simpler model in which the system is embedded in an infinite well.

A. The EPM and the matching conditions

The first step of the method is to compute the complex band structure in each layer of the heterostructure using the Schrödinger equation in $\vec{k}$–space:

$$H^{s,s'}_{\vec{G},\vec{G}'} = \left[\frac{\hbar^2}{2m}(\vec{k}+\vec{G})^2 - E\right]\delta_{\vec{G},\vec{G}'}\delta_{s,s'} + V(\vec{G}-\vec{G}')\delta_{s,s'} - I^{s,s'}_{\vec{G},\vec{G}'}, \quad (1)$$

where $I^{s,s'}_{\vec{G},\vec{G}'}$ represents the spin-orbit term.

The crystal potential is treated as a local pseudo-

potential[8] described in terms of atomic form factors:

$$V(\vec{G}) = \sum_{\alpha} v_{\alpha}(\vec{G}) S_{\alpha}(\vec{G}), \tag{2}$$

where $S_{\alpha}(\vec{G})$ represents the structure factor and $v_{\alpha}(\vec{G})$ the form factors for atom species α.

The spin-orbit term is included in its usual formulation:[9,10,11]

$$\begin{aligned} I^{s,s'}_{\vec{G},\vec{G}'} &= -i \sum_{\alpha} \lambda_{\alpha} S_{\alpha}(\vec{G}-\vec{G}') \\ &\quad \times \left[(\vec{k}-\vec{G}) \wedge (\vec{k}-\vec{G}') \right] \cdot \vec{\sigma}_{s,s'} \\ &= -i\Lambda(\vec{G}-\vec{G}') \left[(\vec{k}-\vec{G}) \wedge (\vec{k}-\vec{G}') \right] \cdot \vec{\sigma}_{s,s'}, \end{aligned} \tag{3}$$

where $\vec{\sigma}$ represents the usual vector of Pauli matrices and λ_{α} the spin-orbit form factors.

In the case of heterostructures the symmetry is retained in the plane perpendicular to the growth direction and the component of the wave vector $\vec{k}$ parallel to this plane is still a good quantum number. $\vec{k}$ may be decomposed into $\vec{k} = (\vec{k}_{\parallel}, k_{\perp})$. The Hamiltonian can be written as a polynomial expansion in $k_{\perp}$:

$$H^{s,s'}_{\vec{G},\vec{G}'} = H^{s,s'}_{2,\vec{G},\vec{G}'} k_{\perp}^2 + H^{s,s'}_{1,\vec{G},\vec{G}'} k_{\perp} + H^{s,s'}_{0,\vec{G},\vec{G}'}, \tag{4}$$

where:

$$\begin{aligned} H^{s,s'}_{2,\vec{G},\vec{G}'} &= \frac{\hbar^2}{2m} \delta_{\vec{G}',\vec{G}} \delta_{s',s}, \\ H^{s,s'}_{1,\vec{G},\vec{G}'} &= \frac{\hbar^2}{m} G_{\perp} \delta_{\vec{G}',\vec{G}} \delta_{s',s} - i\Lambda(\vec{G}-\vec{G}') \vec{A} \cdot \vec{\sigma}_{s',s}, \\ H^{s,s'}_{0,\vec{G},\vec{G}'} &= \left[\frac{\hbar^2}{2m} (\vec{k}_{\parallel}+\vec{G})^2 - E \right] \delta_{\vec{G}',\vec{G}} \delta_{s',s} \\ &\quad + V(\vec{G}-\vec{G}') \delta_{s',s} - i\Lambda(\vec{G}-\vec{G}') \vec{B} \cdot \vec{\sigma}_{s',s}, \end{aligned} \tag{5}$$

where we have used the definitions:

$$\vec{A} = \hat{k}_{\perp} \wedge (\vec{G}-\vec{G}'), \tag{6}$$

$$\vec{B} = \vec{k}_{\parallel} \wedge (\vec{G}-\vec{G}') + \vec{G}' \wedge \vec{G}. \tag{7}$$

It can be shown[12,13] that this equation may be recast as an eigenvalue problem in $k_{\perp}$ for fixed energy, $k_{\parallel}$ and growth direction.

This eigenproblem gives all the required information, namely all the $k_{\perp}$ and the corresponding eigenvectors, to allow the wavefunction to be completely determined.

If a complex band structure is determined for adjacent layers i and $i+1$, with an appropriate band offset, regular matching conditions can be imposed as:

$$\Psi_i(\vec{r}) = \Psi_{i+1}(\vec{r}), \tag{8}$$

$$\frac{\partial \Psi_i}{\partial z}(\vec{r}) = \frac{\partial \Psi_{i+1}}{\partial z}(\vec{r}), \tag{9}$$

at the interface between layers. These conditions can be re-expressed as matrix conditions connecting the wave functions in both layers. A predetermined wavefunction in the first layer results then in fixed coefficients across the structure.

B. The infinite well models

Using the matching conditions and the complex band structure information from last section it is simple to fix infinite well conditions at the extremities of the structure. Denoting by 0 the left interface for the first layer and by N the right interface for the end layer we shall have:

$$\Psi_0 = \Psi_N = 0. \tag{10}$$

These conditions in conjunction with the matching conditions form a set of equations whose solution is usually expressed as a determinant.[14] Determining the solution is however best tackled by singular value decomposition techniques. With this approach it is easy to determine all the energy levels for the system by analyzing the behavior of the singular values.

It should nevertheless be mentioned that the method still suffers from all the problems described previously.[14]

C. The Empirical Pseudopotential Layer Method

The EPLM is far more general than the infinite well models. The numerical problems inherent in that method are not present and appropriate boundary offsets and materials can be selected.

Using the complex band structure information and the matching techniques a scattering matrix approach may be implemented.[15,16] The energy levels are determined by analyzing the resonances of the transmission coefficient across the structure. By calculating the wavefunctions at those energies all properties are then accessible.

This method is extremely well suited to the study of general heterostructures as no assumptions need be made about its layout or its growth direction. The band offsets between layers are taken from experimental values.

D. Wavefunction based calculations

Both methods give enough information, after an initial energy level determination, to compute the wavefunction or any other observables. In fact for a fixed growth direction, energy and parallel wavevector the methods supply a complete description of the wavefunctions. This information is then used to compute the relevant properties.

In particular we compute the parallel averaged probability density, given by:

$$\rho(r_{\perp}) = \int d^2 r_{\parallel} \Psi^{\dagger}(\vec{r}) \Psi(\vec{r}), \tag{11}$$

which can then be used to compute the total probability density:

$$P = \int dr_{\perp} \sigma(r_{\perp}). \tag{12}$$

Another useful quantity is the parallel averaged spin polarization given by:

$$\bar{\sigma}_i(r_\perp) = \int d^2 r_\parallel \Psi^\dagger(\vec{r})\sigma_i\Psi(\vec{r}), \tag{13}$$

which will then give a total spin polarization of the form:

$$\bar{\sigma}_i = \frac{\int dr_\perp \bar{\sigma}_i(r_\perp)}{P}. \tag{14}$$

The method is flexible enough to compute any other relevant observable if necessary.

III. SYMMETRIES

A. Basic definitions

Let us start by firmly setting the scope of our work. We are interested in the spin physics of lattice matched heterostructures of diamond–like and zincblende materials.

In the possible plethora of all these structures it is useful to separate them into categories. Firstly we consider the atomic layer layout. If these structures have a mirror symmetric atomic layer distribution we say it is a symmetric structure. Examples of these are often used and include, for instance, layouts of GaAs in AlAs.

We have to stress that although the atomic layer layout may be symmetric the atomic positions within the layers are such that the layers are not strict mirror images of each other.

Any layout that is not symmetric is said to be asymmetric.

Another useful classification considers the sharing or not of a common anion in the structure. The case of GaAs in AlAs is a clear case of a common–anion structure. There are however situations where this does not happen. For example, a heterojunction of GaSb and InAs is such a case. This is then said to be a no–common–anion structure.

These definitions will later become important in characterizing the symmetries of the structures.

B. Symmetries

For bulk semiconductors the spin splittings are determined by the symmetry of the crystal lattice. Diamond has point group O_h and zincblende T_d. These determine which terms are allowed in the Hamiltonian, whether the spin splittings are possible and, in that case, which form they have.

In the case of heterostructures the symmetry is reduced and it is important to know which subgroup of the bulk group a particular structure has. It is however impractical to enumerate all the point groups for every possible layout and every possible growth direction. We confine ourselves therefore to the most common cases.

In the case of diamond–like materials the most usual layouts consist of layers of Si and Ge grown in the [001] direction. In symmetric configurations these structures have either point group D_2d or D_2h. An odd number of atomic layers of one embedded in the other has point group D_2d while an even number has point group D_2h.

Non ideal interfaces containing monatomic fluctuations can also produce structures with point groups C_2v, C_4v and D_4h.[6] We shall however not consider these cases as the methods used in this work can only handle perfect interfaces.

In the case of zincblende heterostructures with a common anion grown in the [100] direction we conclude that symmetric structures have point group D_2d while asymmetric structures have point group C_2v. For structures without a common anion we have point group C_2v.

A summary of these cases is given in table I.

Diamond [001]	Symmetric	odd number of atomic layers	D_2d
		even number of atomic layers	D_2h
	Asymmetric		C_2v
Zincblende [001]	Symmetric	Common-anion	D_2d
		No common-anion	C_2v
	Asymmetric		C_2v

TABLE I: Summary of point groups for heterostructures grown in the [001] direction.

However, these considerations only provide us with a rule–of–thumb. The point group of a particular heterostructure must be determined for that particular case. Many arrangements with only slight alterations can be produced which have different point groups. For other growth directions similar considerations apply but the resulting point groups will generally be different.

C. Symmetries and the Hamiltonian

In any particular situation we can always consider the Hamiltonian as an expansion in powers of $\vec{k}_\parallel$ about a high symmetry point in the 2D Brillouin zone, usually Γ. Indeed this is the basis of the popular $\vec{k}\cdot\vec{p}$ approximation. The particular terms we are interested in are those involving spin of the form:

$$\gamma_{\alpha,\beta,\cdots,\zeta,\cdots}\sigma_\alpha k_\beta\cdots k_\zeta\cdots, \tag{15}$$

where $\gamma_{\alpha,\beta,\cdots,\zeta,\cdots}$ is a case dependent constant, σ_α one of the Pauli matrices and the $k_\beta\cdots k_\zeta\cdots$ a product of components of the $\vec{k}_\parallel$ vector.

Most of these terms are not allowed by symmetry and may be excluded. In fact, when we are interested in the behavior near an extremum such as the Γ point, it is usually sufficient to consider the first few terms.

In the case of diamond–like structures with point group D_{2h} no spin-orbit terms of the form (15) are allowed in the Hamiltonian and hence no spin splittings should be observed. This is easily understood as this point group has as a constituent symmetry the inversion center.

In the case of the point group D_{2d} this is however not the case. Linear terms like:

$$\sigma_x k_x - \sigma_y k_y, \tag{16}$$

are possible and thus linear splittings may be observed.

This linear contribution can be understood in terms of the cubic terms[17,18,19] in the bulk and has hence been coined the Dresselhaus or bulk inversion asymmetry (BIA) term.

A simple toy model can be constructed with this term and it is easy to calculate the spin polarization as a function of $\vec{k}_{\|}$. This dependence for a fixed magnitude of $\vec{k}_{\|}$ plotted at regular angular intervals will henceforth be called a spin diagram. For this particular case the two possible spin diagrams are displayed in figure 1.

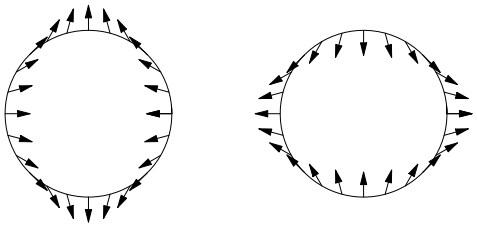

FIG. 1: Spin diagrams for the Dresselhaus contribution. Magnitude of spin scaled for clarity.

In the case of a structure with C_{4v} the only invariant that can be found is the term:

$$\sigma_x k_y - \sigma_y k_x, \tag{17}$$

which again allows for linear splittings. This contribution was understood early by Rashba[20,21] in terms of the consequences of structural asymmetry in the material. This term is usually called the Rashba or structural inversion asymmetry (SIA) term.

The toy model can be repeated with the Rashba term and its characteristic spin diagram is depicted in figure 2.

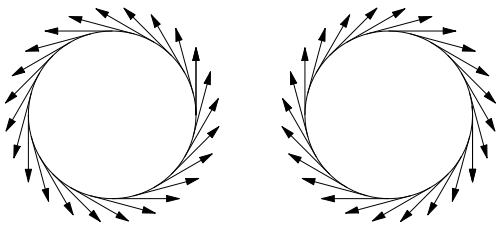

FIG. 2: Spin diagrams for the Rashba contribution. Magnitude of spin scaled for clarity.

The determination of the spin diagrams is an easy method to visualize the symmetries as these act as symmetry signatures.

For point group C_{2v} both BIA and SIA terms are allowed and the spin diagram looks like a superposition of both. An example is shown in figure 3.

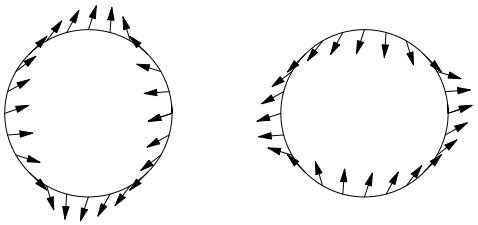

FIG. 3: Spin diagrams for a particular case of mixed BIA and SIA contributions. Magnitude of spin scaled for clarity.

In this situation the angle of the spin direction at $\vec{k}_{\|} = (k_x, 0)$ with the [100] direction is a good measure of the degree of mixing.

The zero–field spin splittings may be represented[17] by an effective magnetic field. This will produce a spin Hamiltonian term of the form:

$$H = \frac{1}{2}\hbar\vec{\sigma}\cdot\vec{B}_{\rm eff}(\vec{k}_{\|}), \tag{18}$$

where $\vec{B}_{\rm eff}(\vec{k}_{\|})$ will depend on the magnitude and direction of the parallel wavevector $\vec{k}_{\|}$. From this Hamiltonian we obtain an overall spin splitting given by:

$$\Delta(\vec{k}_{\|}) = \hbar\left|\vec{B}_{\rm eff}\right|. \tag{19}$$

From our previous discussion we can already deduce that $\vec{B}_{\rm eff}$ will have two contributions: the bulk term (BIA) and a structural term (SIA).

In the case of bulk zincblende structures this term produces a well known contribution[17,19] for small values of $\vec{k}$ of the form:

$$\vec{B}_{\rm eff} = \frac{2\gamma}{\hbar}\left[k_x(k_y^2 - k_z^2)\hat{x} + k_y(k_z^2 - k_x^2)\hat{y} + k_z(k_x^2 - k_y^2)\hat{z}\right] \tag{20}$$

where γ is a material dependent constant. In the case of our structures this has been shown[17,18] to simplify to the form:

$$\vec{B}_{\rm BIA} = \frac{2\gamma}{\hbar}(k_{z,w}^2)(-k_x\hat{x} + k_y\hat{y}), \tag{21}$$

where $k_{z,w}$ is the value of the confined wavevector in the well. This term is exactly the one predicted by symmetry and will produce a spin splitting $\Delta_{\rm BIA}$, that is linear in $\vec{k}_{\|}$ and isotropic.

In the case of structural inversion asymmetry it was shown[20,21] that this effective field is:

$$\vec{B}_{\rm R} = \frac{\alpha}{\hbar}(\vec{k}\wedge\hat{k}_{\perp}), \tag{22}$$

where $\hat{k}_\perp$ is just the unit vector in the growth direction. For the particular case of the [001] growth direction this is then:

$$\vec{B}_{\rm R} = \frac{\alpha}{\hbar}(k_y\hat{x} - k_x\hat{y}). \tag{23}$$

The spin splitting for this case $\Delta_{\rm R}$, is again linear in $\vec{k}_\parallel$ and also isotropic.

In the general case where both terms can co-exist a total spin splitting is given by:

$$\Delta(\vec{k}_\parallel) = \hbar\left|\vec{B}_{\rm BIA} + \vec{B}_{\rm R}\right|, \tag{24}$$

which can be expressed as:

$$\Delta(\vec{k}_\parallel) = \sqrt{\Delta^2_{\rm BIA} + \Delta^2_R - 2\Delta_{\rm BIA}\Delta_R\sin(2\theta)}, \tag{25}$$

where θ is the angle between $\vec{k}_\parallel$ and the [100] direction. In general this spin splitting is linear in $\vec{k}_\parallel$ but anisotropic.

D. Symmetries and the simulation methods

Both models used in this work, the infinite well models and the Empirical Pseudopotential Layer Method, contain atomistic information about the structure under consideration and should hence reproduce the full symmetries of the cases under study. There are however some practical but soluble problems.

Firstly it should be noted that the method uses only integer numbers of monolayers (i.e. pairs of atomic layers) which takes some cases out of our reach. An obvious example is the single layer of Si in Ge. As this restriction only comes about as a simplification in the matching technique it is possible to remove it if any of the cases in this category becomes important.

Another problem concerns simulations with common atoms across different material layers. We should remember that the Empirical Pseudopotential Method uses form factors determined for each material individually and hence the common atom is described by different potentials in different layers. This may cause a further reduction in the symmetry which is visible in the results but, as we shall see, does not invalidate them. A change to consistent atomic form factors would only partially solve this problem. Even if the same form factors are used for the common atom, and because the algorithm forces us to use integer number of monolayers, we would have one atomic layer of these anions at a different offset. However if we solve the matching at integer number of atomic layers this problem would also be solved.

A few notes on the particular simulation cases chosen are appropriate at this stage. As a simulation method the Empirical Pseudopotential Method is quite robust and powerful because the layout of the heterostructure is completely arbitrary: the growth direction, the number of layers, which materials and which band offsets are all set as input. This much freedom allows simulations with structures whose layout is completely artificial. These cases are however as important as those of naturally occurring heterostructures. If the latter give us precious data comparable with experimental results the former enable us to explore every possible dependence on the heterostructures' defining characteristics by carrying out computer experiments which would not be possible in a real laboratory.

We should note that the artificial cases considered are not so far from physical situations that render then absurd. For example the infinite well situations are attainable by using wide gap materials or even insulators to confine the system. Varying band offsets is also feasible to some extent by using alloying techniques.

IV. DIAMOND HETEROSTRUCTURES

For the crucial case of diamond heterostructures we have used two distinct simulations. First we considered the case of a layer of Ge in infinite walls. This structure should also have point group $D_{2\rm h}$ and no spin splittings should arise. The second case is that of a layers of Ge in Si with an artificial offset to produce a well for holes in the intermediate layer. This situation also has point group $D_{2\rm h}$ and no spin splittings should be observed. We should point out that strain effects at the interfaces have been completely ignored. The two physical situations are represented in figure 4.

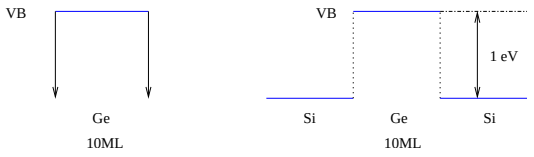

FIG. 4: Well layouts for diamond-like structures. The layout on the left represents 10 monolayers of Ge in infinite walls under the valence band while the right layout represents 10 monolayers of Ge in Si with an artificial offset to produce a 1 eV deep well adjusted on the valence band edges.

Both simulations were run on extremely small energy grids and the results showed no spin splittings at all as we can see in figures 5 and 6 for the two situations. In the second situation it should be noted that the two very close energy levels correspond to two twofold degenerate energy levels and not to one energy level displaying spin splitting. This was verified by a computation at the Γ point were the energy levels are close but not degenerate.

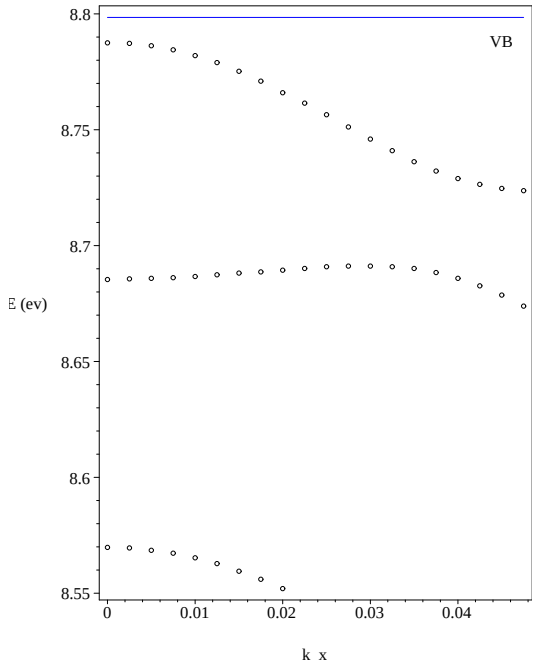

FIG. 5: Energy dispersion for the well layout represented on the left of figure 4. $\vec{k}_{\|} = (k_x, 0)$ in units of $\left(\frac{2\pi}{a}\right)$ Å^{-1}. VB represents the valence band edge of Ge.

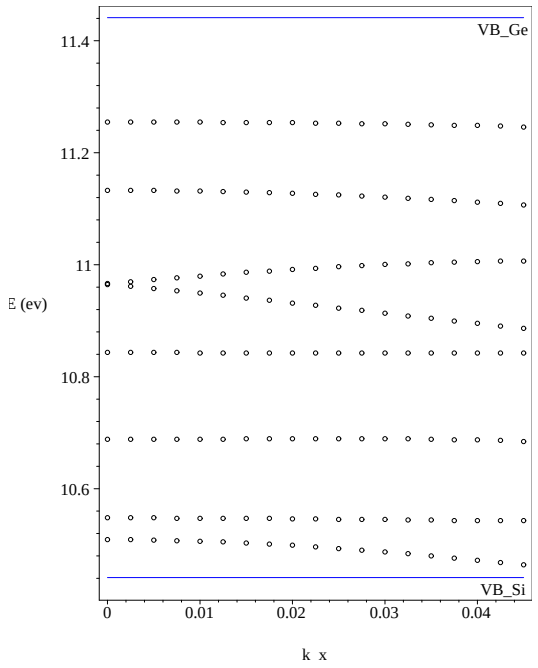

FIG. 6: Energy dispersion for the layout represented on the right of figure 4. $\vec{k}_{\|} = (k_x, 0)$ in units of $\left(\frac{2\pi}{a}\right)$ Å^{-1}. VB_Ge represents the valence band edge of Ge and VB_Si the valence band edge of Si.

These results are hence in line with our predictions.

Some claims have been put forward[6] that in principle we could engineer spin splittings by producing a structure with a point group different from D_{2h}. As we have established, this corresponds to the case of an odd number of atomic layers in the well. This situation is also extremely interesting: although bulk diamond–like structures do not show any spin splittings, and hence the Dresselhaus term cannot be present, in the case of heterostructures this term is present. It is hence possible to have spin splittings originating from a Dresselhaus contribution even if the terms are absent in bulk material. There is then an alternative way to engineer spin splittings in these structures which does not rely on the Rashba effect. However this case is out of the reach of our simulation methods in their current form.

There are nevertheless other ways. To show that spin splittings can indeed be achieved in structures involving diamond–like materials we tested two situations that break inversion symmetry. The first is a sandwich of two layers, one of Si and the other of Ge, in infinite walls with an appropriate offset to line up the valence band edges. The second consists in the artificial case of Ge sandwiched between layers of Ge but with an artificial asymmetric offset. These cases do not have point group D_{2h} and do not have an inversion center; spin splittings are therefore allowed. Both situations are represented in figure 7.

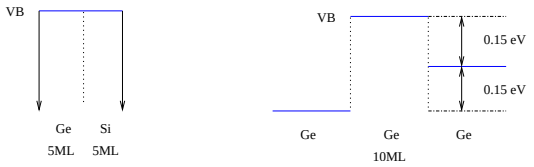

FIG. 7: Well layouts for diamond-like structures. The layout on the left represents 5 monolayers of Ge and 5 monolayers of Si in infinite walls with lined-up valence bands while the right layout represents 10 monolayers of Ge in Ge with artificial asymmetric offsets.

The resulting energy dispersions for these two situations are in figures 8 and 9 respectively.

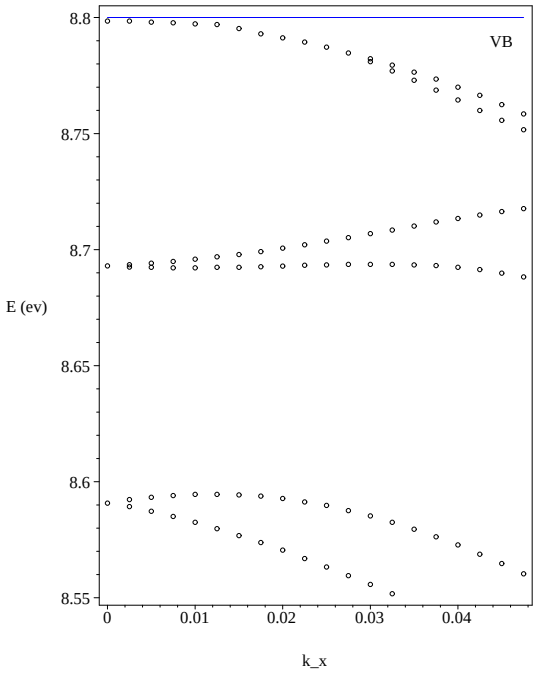

FIG. 8: Energy dispersion for the well layout represented on the left of figure 7. $\vec{k}_{\|} = (k_x, 0)$ in units of $\left(\frac{2\pi}{a}\right)$ Å^{-1}. VB represents the artificially set common valence band edge.

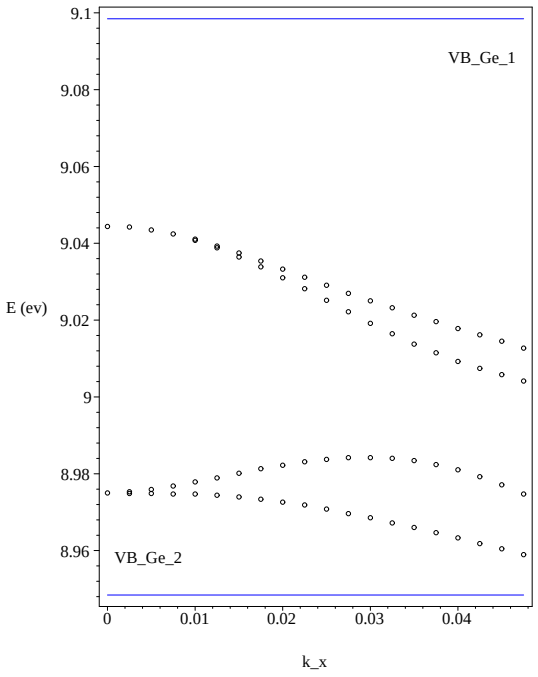

FIG. 9: Energy dispersion for the well layout represented on the right of figure 7. $\vec{k}_{\|} = (k_x, 0)$ in units of $\left(\frac{2\pi}{a}\right)$ Å^{-1}. VB_Ge_i represents the artificially set valence band edges for the i^{th} layer.

As we can see spin splittings are apparent in both situations and hence these materials show potential for spintronic devices.

The situation of infinite potential at the boundaries is also a case of perfect symmetric confinement. In this situation no extra asymmetry, other than the crystal potential, can cause the spin splittings and only an interplay between crystal potential and confinement is responsible for them. This case may be described as spin splitting enhancement by symmetric confinement and would have occurred even if a single zincblende compound had been used, as we shall see later. This enhancement refers to values of spin splitting far bigger than those observed in bulk.

Two main conclusions may be drawn. Firstly, the two simulation methods we have used are perfectly capable of handling situations where by symmetry no spin splitting is possible. Secondly, and more importantly, even in the case of materials where a center of inversion is present structures can be engineered which have spin splittings. This is of the utmost importance as Si and Ge are presently the basis of most of the semiconductor industry.

V. ZINCBLENDE COMMON-ANION HETEROSTRUCTURES

The case of symmetric structures is still somewhat controversial in the literature. Most of this controversy stems from the fact that the conventional model of electronic structure in heterostructures, the $\vec{k} \cdot \vec{p}$ method, does not fully account for their symmetries. In fact, in this method the wavefunctions are expanded in a set of Γ Bloch states of the zincblende crystal. Further this expansion is restricted to a few states, usually the top of the valence band and the bottom of the conduction band. With this set it is impossible to resolve any atomistic details and the method is incapable of reproducing the correct point group symmetries of the structure. This was thought not to be problematic given the small values of the bulk terms from BIA. However, work[18] as early as 1988 hinted that this is not the case. More recent theoretical studies[5] have confirmed this. Nevertheless all these studies rely on introducing terms in the $\vec{k} \cdot \vec{p}$ model that mimic the symmetries of the structure under consideration and have thus to be tailored to particular situations. In contrast any atomistic approach, like the Empirical Pseudopotential Method, incorporates by construction the correct symmetry of the structure. However no such calculations, or even experimental data, is, to our knowledge, available for the case of spin splittings. It should also be noted that in this particular case, zincblende common-anion structures, no structural asymmetry is introduced and any spin splitting cannot be attributed to the Rashba effect.

Given that linear or cubic terms exist in bulk it is expected that any band would split linearly close enough to the Γ point. The fact that the point group of these

structures with a common-anion D_{2d} allows these terms further reinforces our belief that this must indeed happen. Nothing however tells us that the coefficient associated with this phenomenon would be big enough to allow eventual technological use of these structures. Nevertheless the case of spin splitting enhancement by symmetric confinement that we have already encountered lets us believe that this is the case.

A first introductory calculation with GaSb in infinite walls is then performed. The band edge layout for this structure is depicted on the left of figure (10). The energy dispersion computed with the infinite well model is represented in figure 11.

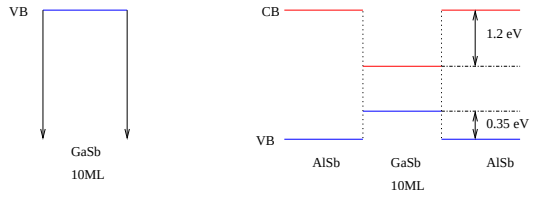

FIG. 10: Well layout for zincblende structures. The layout on the left represents 10 monolayers of GaSb in infinite walls under the valence band while the right layout represents a well of 10 monolayers of GaSb in AlSb.

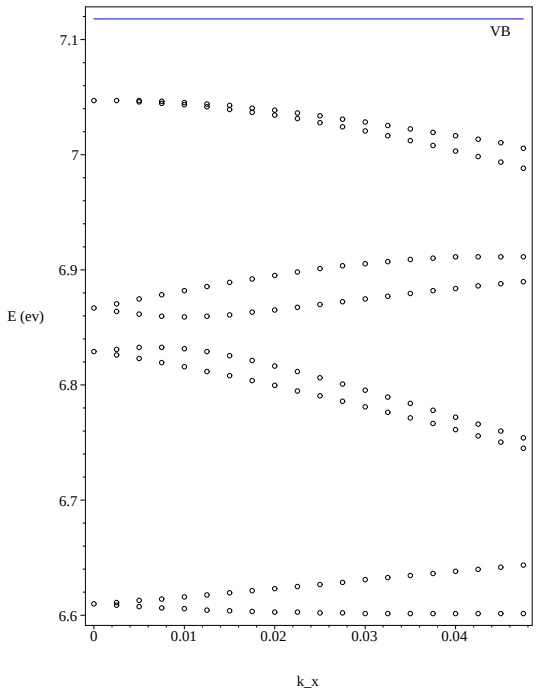

FIG. 11: Energy dispersion for the layout represented on the left of figure 10. $\vec{k}_{\parallel} = (k_x, 0)$ in units of $\left(\frac{2\pi}{a}\right)\text{Å}^{-1}$. VB represents the valence band edge of GaSb.

Again we clearly see spin splittings that far exceed typical values of bulk spin splittings. This is then another case of symmetric confinement enhancement of the spin splittings. It should be noted that for this particular direction there is no spin splitting in the bulk case.

A more realistic case of GaSb sandwiched between AlSb was also used. The band layout is depicted on the right of figure 10 where the band offsets were set to acknowledged experimental values.[22]

The computed energy dispersions for both the conduction and valence band energy windows is shown in figures 12 and 13 respectively.

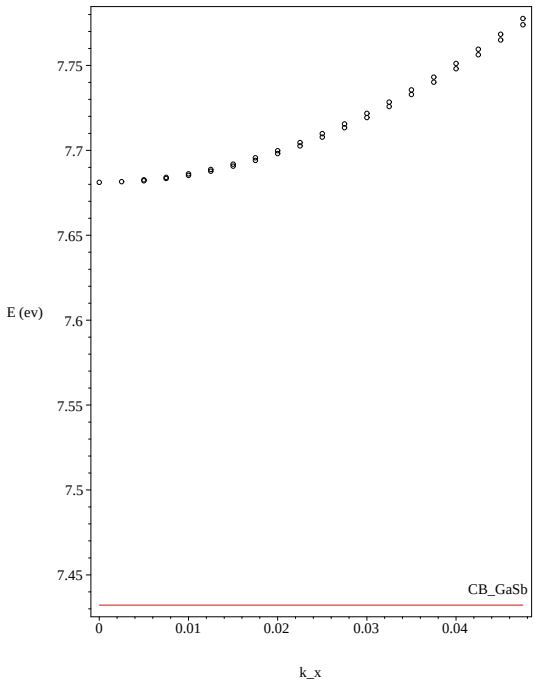

FIG. 12: Energy dispersion for the layout represented on the right of figure 10 for the energy window of conduction band. $\vec{k}_{\parallel} = (k_x, 0)$ in units of $\left(\frac{2\pi}{a}\right)\text{Å}^{-1}$. CB_GaSb represents the conduction band edge of GaSb.

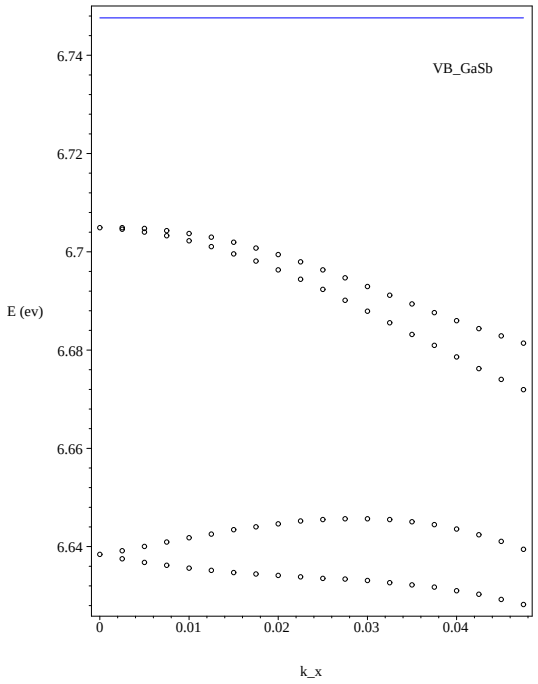

FIG. 13: Energy dispersion for the layout represented on the right of figure 10 for the energy window of the valence band. $\vec{k}_{\|} = (k_x, 0)$ in units of $\left(\frac{2\pi}{a}\right)$Å^{-1}. VB_GaSb represents the valence band edge of GaSb.

Every band is clearly spin split: a fact that can be confirmed by a calculation of the spin polarization. As before, for the [001] direction no spin splitting is observed in the bulk case. In both the conduction and valence band the spin splitting can be easily fitted to a linear dispersion, $\Delta E \propto k$, yielding a coefficient of 76.5 meV Å and 196.58 meV Å respectively.

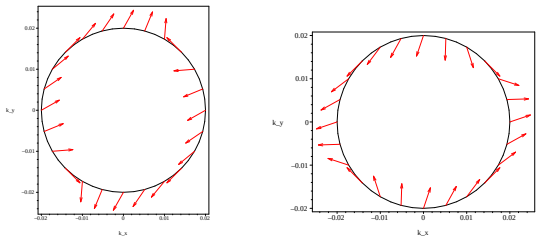

FIG. 14: Spin diagram for the first conduction level (left) and valence level (right) in the band structure of figures 12 & 13 respectively with $k_{\|} = 0.02\left(\frac{2\pi}{a}\right)$Å^{-1}. $\vec{k}_{\|} = (k_x, k_y)$ in units of $\left(\frac{2\pi}{a}\right)$Å^{-1}. Magnitude of spin scaled for clarity.

The spin diagrams for a fixed $k_{\|} = 0.02\left(\frac{2\pi}{a}\right)$Å^{-1} and computed for the first energy level on the energy windows for the conduction and the valence bands are shown in figure 14. They represent a clear signature of the Dresselhaus terms and cannot be attributed to any structural inversion asymmetry. The slight deviation from the perfect D_{2d} signature was already explained in section III D. In this case the spurious Rashba term is approximately 0.34 times the Dresselhaus contribution. It should be noted that the z component of the spin polarization is always found to be zero within numerical fluctuations. Spin diagrams for other energy levels were computed with similar results.

It is important to note the values of the linear coefficients. These values are comparable to the linear coefficients stated in literature[23] for the Rashba coefficient in asymmetric structures. It should also be noted that these values cannot be attributed to the spurious Rashba contributions in this case. The situation with infinite walls does not suffer from this contamination and produces similar results. This fact alone is technologically important: structural asymmetry is probably not required to produce structures that behave similarly to those currently proposed for the purpose of creating spin splittings. The spin behavior as shown in the spin diagrams is completely different, however.

As the SIA and BIA contributions have similar magnitudes it is important that both are included in any study. This is particularly important when methods, such as $\vec{k}\cdot\vec{p}$ are employed, which don't automatically contain Dresselhaus contributions. Even when the Rashba contribution is important the interplay of the 2 terms may produce sizable effects.

Another major achievement of this method is the possibility of extracting atomistic details in clear contrast to the majority of the methods previously used. In figure 15 the parallel averaged probability densities for the first energy level in the valence band energy window is depicted.

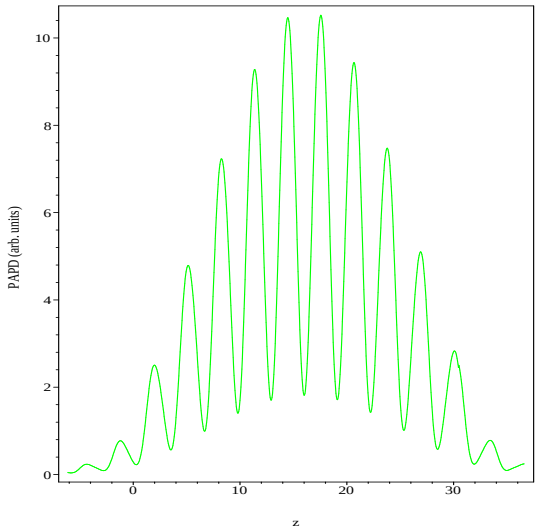

FIG. 15: Parallel averaged probability density for the first energy level in the energy window of the valence band, as depicted in figure 12 for $\vec{k}_{\|} = (0.02, 0)\left(\frac{2\pi}{a}\right)$Å^{-1}. Horizontal axis corresponds to the growth direction in Ångström.

Clearly the general trend is the same as in previous cal-

culations but a wealth of extra information is portrayed. The general belief that the envelope behaves as predicted by "particle-in-box" type calculations is confirmed even in this atomistic calculation. Also displayed clearly is that there are deviations from the envelope behavior in the atomistic detail of these graphs. This could help engineer particular structures tailored to exhibit particular physical effects or even in the determination of the best doping technique. Similar results are obtained for all other energy levels.

Atomistic detail is also clear in the parallel averaged spin polarization. This is depicted in figure 16 corresponding to the parallel averaged probability density depicted in figure 15. This level of detail in spin behavior can be important in tailoring particular spin properties and possibly in doping with magnetic materials.

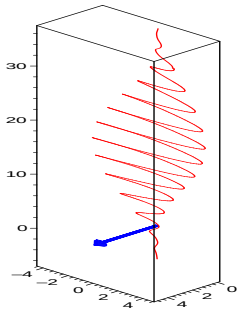

FIG. 16: Three-dimensional representation of the parallel averaged spin polarization $\vec{\sigma}(r_\perp) = (\overline{\sigma}_x, \overline{\sigma}_y, \overline{\sigma}_z)$, corresponding to the parallel averaged probability density in figure 15. Vertical axis corresponds to the growth direction in Ångström. The continuous line corresponds to following the tip of the vector $\vec{\sigma}(r_\perp)$ in space after appropriate scaling. The arrow is a vector in the direction of $\vec{k}_\parallel$ introduced as guidance.

It should be noted that most of the atomistic detail, in the particular case of the Dresselhaus term, is in a plane perpendicular or nearly perpendicular to $\vec{k}_\parallel$. It's however the component parallel or nearly parallel to $\vec{k}_\parallel$ that averages to the total spin polarization in accordance to the spin diagrams characteristic of this term. This atomistic detail of the spin polarization has never been reported previously.

It is also possible to use known data from bulk materials to compare with our results. We know that for the conduction band spin splittings are given by cubic terms originating in the Hamiltonian term given by equation (20). The constant γ can be obtained in the literature[24] and values range from 109.4 to 153.9 eV Å^3 for theoretical predictions with several methods and 186.3 eV Å^3 for the experimental value. In the case of GaSb in AlSb the spin splittings of the levels in the conduction band energy window should then originate, to first approximation, in linear and quadratic terms in $k_{z,w}$, the value of the confined wavevector. For wide enough wells this value should be, for the first energy level, approximately $\frac{\pi}{L}$, with L the well width given by $\frac{1}{2}aN$ where a is the lattice constant and N the number of monolayers in the well.

A well width dependence for the first electronic energy level was then computed and the result is shown in figure 17.

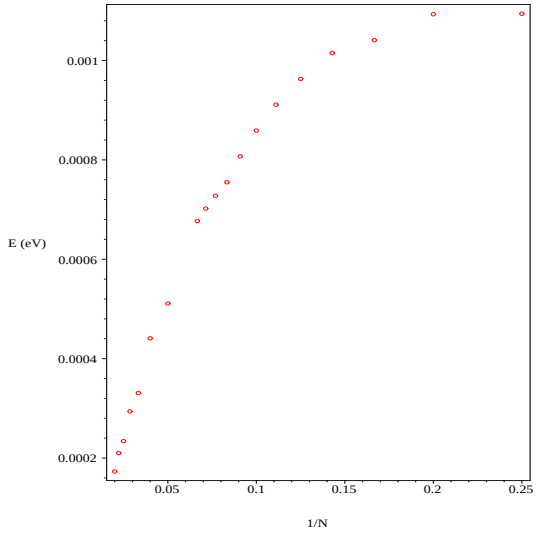

FIG. 17: Spin splitting of the first energy level in the energy window of the conduction band for $\vec{k}_\parallel = (0.01, 0)\,(\frac{2\pi}{a})\text{Å}^{-1}$ as a function of the inverse well width given by the number of monolayers of GaSb.

For the widest wells the linear contribution should be dominant and the spin splitting should behave as:

$$\Delta = \frac{2\gamma\pi k_x^2}{a}\left(\frac{1}{N}\right). \tag{26}$$

A linear fit to this data gives a value of γ of 118.2 eV Å^3.

Given all the approximations used this value is in very good agreement not only with results using very different approaches, but also with experiment, and gives us confidence in the reliability all of the results of the method.

As a final conclusion on this section it should be noted that although our results are for a particular case we believe that the dominant trends in these structures are determined by symmetry and rather than by the particular atoms involved. Further calculations for the case of GaAs in AlAs were also computed and produced similar results.

VI. ASYMMETRIC HETEROSTRUCTURES

In the case of symmetric wells with a common anion we probed the consequences of introducing the Dresselhaus term. As a first approach we would be interested in probing the Rashba contribution in the same way. The case of asymmetric structures grown in the [001] direction is however usually in the C_{2v} point group class which allows

both terms. However we already know that the Dresselhaus term arises from bulk inversion asymmetry. Hence, if we consider a structure with dominant structural inversion asymmetry we should minimize the its effects. For this purpose we revisit the artificial structure of Ge sandwiched between layers of Ge but with asymmetric band offsets as depicted on the right of figure 7. We should nevertheless remember that, even though bulk Ge does not allow the Dresselhaus contribution, this structure will contain this term even if it is small. We have already shown that such contributions occur in cases where the center of inversion has been removed as in the case of the double layer of Si and Ge in infinite walls. However these should be smaller than in any structure constructed out of zincblende materials. As we shall see the Dresselhaus contribution in this case is far smaller than the Rashba term.

The computed energy dispersion in the energy window of the valence band was already displayed in figure 9. The bands clearly show spin splittings which have been confirmed by a calculation of the spin polarization. A linear fit to the actual spin splitting for the first band gives a splitting coefficient of 324.3 meV Å.

This value is of the same order as those calculated for the case of symmetric structures; further reinforcing our conclusion that BIA must always be taken into consideration.

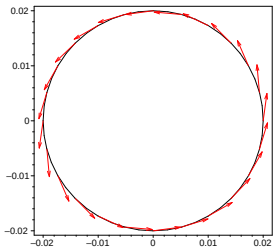

FIG. 18: Spin diagram for the first valence level with $k_{\|} = 0.02\,(\frac{2\pi}{a})\text{Å}^{-1}$. $\vec{k}_{\|} = (k_x, k_y)$ in units of $(\frac{2\pi}{a})\text{Å}^{-1}$. Magnitude of spin scaled for clarity.

More importantly we have also calculated the spin diagram for this case which is given in figure 18. In this case the z-component of the spin polarization is also found to be zero within numerical fluctuations. As we can see it forms a clear signature of the Rashba contribution. The slight deviation is due, in this case, to the Dresselhaus term which is allowed by the symmetry arrangement. This term is approximately 0.14 times the dominant Rashba contribution.

In this situation it is also possible to extract atomistic details from our results. In figure 19 a parallel averaged probability density is shown.

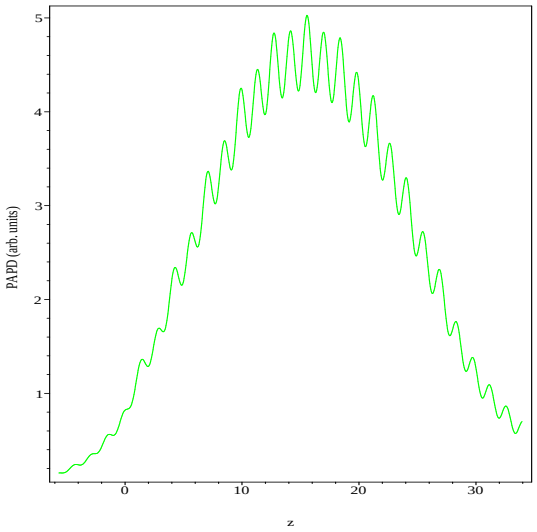

FIG. 19: Parallel averaged probability density for the first energy level in the energy window of the valence band, as depicted in figure 9, for $\vec{k}_{\|} = (0.02, 0)\,(\frac{2\pi}{a})\text{Å}^{-1}$. Horizontal axis corresponds to the growth direction in Ångström.

The typical envelope behavior is reproduced but significantly more information is present. As in the previous case this might be significant for engineering new structures. Atomistic detail is also present in the parallel averaged spin polarizations. This quantity is depicted in figure 20 corresponding to the parallel averaged probability density shown previously.

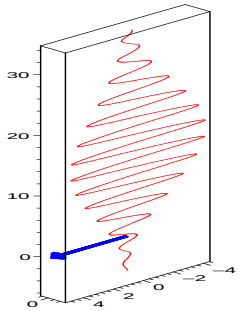

FIG. 20: Three-dimensional representation of the parallel averaged spin polarization $\vec{\sigma}(r_{\perp}) = (\overline{\sigma}_x, \overline{\sigma}_y, \overline{\sigma}_z)$, corresponding to the parallel averaged probability density in figure 19. Vertical axis corresponds to the growth direction in Ångström. The continous line corresponds to following the tip of the vector $\vec{\sigma}(r_{\perp})$ in space after appropriate scaling. The arrow is a vector in the direction of $\vec{k}_{\|}$ introduced as guidance.

This case is different from the case of the Dresselhaus term. Most of the atomistic detail is in the direction of $\vec{k}_{\|}$ while the perpendicular component averages to the total spin polarization in accordance to the spin diagrams characteristic of the Rashba term. Again this level of atomistic detail has never been reported previously.

The main conclusion of our calculations is that structural asymmetry in the system introduces a new term in the Hamiltonian that allows linear splittings close to the Γ point in perfect agreement with the Rashba effect. It is also important to emphasis that the Empirical Pseudopotential Method is capable of simulating this situation.

It is possible to minimize the BIA contribution by using diamond-like materials rather than producing structures with point group C_{4v}. However in a general case both terms will interplay and the magnitude of the Dresselhaus contribution can be comparable to that of the Rashba term. A detailed treatment of these structures must always incorporate both to guarantee an accurate description of the physical processes. This was previously discussed in the literature[5] using the independent $\vec{k} \cdot \vec{p}$ method.

VII. CONCLUSIONS

We have shown that the phenomenon of spin splittings in heterostructures can be put into a consistent global framework. Until now the physics of symmetric and asymmetric structures was thought to be in essence different. We have proven that they are however just different expressions of the same underlying physics: "symmetry rules".

The Empirical Pseudopotential Layer Method is very well suited for atomistic detailed calculations for these structures. It can accurately predict the energy levels and their spin splittings throughout the Brillouin zone. The case of the neighborhood of the Γ point, specifically analyzed in this chapter due to its technological importance, is just a particular case. The method can also play a crucial role in determining both transport and optical properties of these structures as the wavefunction for every possible state is easily obtained. It is also flexible enough to handle arbitrary growth directions and automatically incorporating the correct symmetries, in contrast to the $\vec{k} \cdot \vec{p}$ method which requires to be adapted for each particular symmetry case.

Our most significant conclusion is that in all the studied structures linear terms emerge in the spin splittings. These terms play a crucial part in determining the top or bottom of bands near the Γ point and are usually the determining factor in experimental results that probe close to that point.

The results involving diamond-like materials also provide substantial conclusions. Although bulk materials with this structure do not exhibit spin splittings we proved that heterostructures with these materials may exhibit them. This is of crucial importance as most of today's semiconductor industry is based on Si and Ge. The technology is still not capable of producing structures with absolute layer precision and so the case of odd number of atomic layers is probably unlikely to be of use. However this apparent technological problem can actually be explored to produce interface roughness that is responsible for lowering of symmetry; thus making spin splittings possible[6].

Symmetric structures with a common anion exhibit linear splittings comparable to those determined in asymmetric structures but with different spin behavior. The new field of spintronics may find this new degree of freedom technologically useful. The combination of both Dresselhaus and Rashba may be used to modulate a particular spin behavior.

Our results are in good agreement with the most recent theoretical study[5] in the literature. All linear coefficients for both valence and conduction bands are similar even though the methods used are different. The conclusion that both BIA and SIA must always be included in every calculation is also drawn there.

Comparison with experiment is more difficult, however. Firstly there is a lack of results for the diamond-like structures and for the zincblende symmetric common-anion cases due to the relevance always given to the asymmetric case. Secondly, even for the case of asymmetric structures, it has emerged recently that the most common experimental procedure, using Shubnikov-de Haas oscillations, might not have been properly analyzed[25]. Neveretheless the values obtained[23] are of the same order of magnitude.

There is also another indirect experimental result that can be related to our prediction. An in-plane polarization anisotropy is observed[4] in the case of structures of C_{2v} point group relevant to optical considerations involving interband transitions[26]. This anisotropy reveals itself in the band structure of these heterostructures by a clear difference between the [110] and the $[\bar{1}10]$ directions. This difference is visible in our computed band structures for the asymmetric case. For the common-anion symmetric situation no appreciable difference could be detected. This effect is clearly important for optical devices and can also be determined by the Empirical Pseudopotential Method.

Another point usually considered[5] in the context of spin splittings in heterostructures is the influence of the main gap on the relative magnitude of both contributions. This claim states that in narrow gap systems SIA effects dominate while for wide band gaps BIA is larger. Although we do not have enough data to compare linear coefficients for narrow and large band gaps our results are enough to conclude that even in narrow gap systems, like GaSb, both contributions should be taken into consideration. We consider this claim to be an oversimplification of the dependence of spin splittings on the parameters of the structure. These will depend in a non-simple way not only on the main gap but also on the well width, depth and applied fields. Results obtained[5] elsewhere seem to confirm this.

The results presented here are the first, to our knowledge, atomistic simulations that show that the full spin-orbit interaction caused by the atomic cores is the dominant contribution for the zero-field spin splittings. The particular symmetry of the case under consideration de-

termines the possible behavior: Dresselhaus or Rashba.

---

* Present Address: Department of Physics, Trinity College, Dublin 1, Ireland; Research supported by the FCT (Portugal) under grant PRAXIS XXI/BD/13349/97.; Electronic address: m.a.oliveira@tcd.ie

† The authors wish to acknowledge the contribution of the late Prof. E. A. Johnson to this work.

[1] D. D. Awschalom, M. E. Flatté, and N. Samarth, Scientific American (2002).

[2] S. Datta and B. Das, Applied Physics Letters **56**, 665 (1990).

[3] K. C. Hall, W. H. Lau, K. Gündoğdu, M. E. Flatté, and T. F. Boggess, *Non-magnetic semiconductor spin transistor* (2003), arxiv:cond-mat/ 0307687.

[4] S. D. Ganichev, *Spin-galvanic effect due to optical spin orientation* (2003), arxiv:cond-mat/0303193.

[5] X. Cartoixà, D. Z.-Y. Ting, and T. C. McGill, *Bulk inversion asymmetry effects on the band structure of zincblende heterostructures in an 8-band effective mass approximation model* (2002), arxiv:cond-mat/0212394.

[6] L. E. Golub and E. L. Ivchenko, *Interface-induced electron spin splitting in SiGe heterostructures* (2003), arxiv:cond-mat/0302308.

[7] A. R. Rundell, G. P. Srivastava, and J. C. Inkson, Physical Review B **55**, 5177 (1997).

[8] M. L. Cohen and J. R. Chelikowshy, *Electronic structure and optical properties of semiconductors*, Springer Series in Solid-State Sciences 75 (Springer-Verlag, Berlin, 1989).

[9] G. Weisz, Physical Review **149**, 504 (1966).

[10] S. Bloom and T. K. Bergstresser, Solid State Communications **6**, 465 (1968).

[11] S. Bloom and T. K. Bergstresser, Physica Status Solidi **42**, 191 (1970).

[12] J. B. Pendry, *Low Energy Electron Diffraction* (Academic Press, London, 1974).

[13] Y.-C. Chang and J. N. Schulman, Physical Review B **25**, 3975 (1982).

[14] S. Brand and D. T. Hughes, Semiconductor Science and Technology **2**, 607 (1987).

[15] D. Y. Ko and J. C. Inkson, Semiconductor Science Technology **3**, 791 (1988).

[16] D. Y. Ko and J. C. Inkson, Physical Review B **38**, 9945 (1988).

[17] E. A. de Andrada e Silva, Physical Review B **46**, 1921 (1992).

[18] R. Eppenga and M. F. H. Schuurmans, Physical Review B **37**, 10923 (1988).

[19] M. I. D'Yakonov and V. I. Perel, Sov. Phys. JETP **33**, 1053 (1971).

[20] E. I. Rashba, Soviet Physics - Solid State **2**, 1109 (1960).

[21] Y. A. Bychkov and E. I. Rashba, JETP Letters **39**, 79 (1984).

[22] E. T. Yu, J. O. McCaldin, and T. C. McGill, in *Solid state physics: advances in research and applications*, edited by H. Ehrenreich and D. Turnbull (Academic Press, 1992), vol. 46, pp. 1–146.

[23] A. C. H. Rowe, Ph.D. thesis, Imperial College London (2000).

[24] M. Cardona, N. E. Christensen, and G. Fasol, Physical Review B **38**, 1806 (1988).

[25] R. Winkler, S. Papadakis, E. Poortere, and M. Shayegan, in *Advances in Solid State Physics*, edited by B. Kramer (Springer-Verlag, 2001), vol. 41, pp. 211–223.

[26] R. Magri and A. Zunger, Physical Review B **62**, 10364 (2000).